DNA/TNA mesoscopic modeling of melting temperatures suggest weaker hydrogen bonding of CG than in DNA/RNA

Maria Izabel Muniz^a, Hershel H. Lackey^b, Jennifer M. Heemstra^c, Gerald Weber^{a,*}

^aDepartamento de F'ısica, Universidade Federal de Minas Gerais, 31270-901, Belo Horizonte-MG, Brazil ^bDepartment of Chemistry, University of Utah, Salt Lake City, Utah 84112, United States ^cDepartment of Chemistry, Emory University, Atlanta, Georgia 30322, United States

Abstract

TNA/DNA hybrids share several similarities to RNA/DNA, such as the tendency to form A-type helices and a strong dependency of their thermodynamic properties on purine/pyrimidine ratio. However, unlike RNA/DNA, not much is known about the base-pair properties of TNA. Here, we use a mesoscopic analysis of measured melting temperatures to obtain an estimate of hydrogen bonds and stacking interactions. Our results reveal that the AT base pairs in TNA/DNA have nearly identical hydrogen bond strengths than their counterparts in RNA/DNA, but surprisingly CG turned out to be much weaker despite similar stability.

Keywords: DNA/TNA hybrid, Peyrard-Bishop DNA model, DNA/TNA stability, Hydrogen bonds, Stacking interaction.

1. Introduction

TNA (*CI*-L-(3'-2')-threofuranosyl nucleic acid) is a non-natural DNA analog that is capable of forming anti-parallel duplexes with both DNA and RNA [1], and was found to be more stable and resistant to degradation under physiological conditions [2]. Hybridization of DNA/TNA (DT) was found to be similar to that of DNA/RNA (DR) in a number of ways [3], especially the strong dependence of thermal stability on purine/pyrimidine ratio [4]. Another important similarity is the tendency of DT to form A-type helices, similar to what is found in DR [5, 6]. These similarities have led to discussions if TNA could have been the natural precursor of RNA [7, 8].

^{*}Corresponding author

The sugar moiety in TNA contains carbon atoms and a single oxygen atom, and the phosphodiester groups are linked to the 2¹ and 3¹ positions of the threofuranose ring, as a result its backbone is shorter than that of DNA [9]. Nuclear magnetic resonance (NMR) and X-ray experiments largely confirmed the tendency of DT hybrids to form A-type helices [9–11]. This is hypothesized to result from the ability of DNA to adjust its conformation to TNA, reducing the inter-phosphate distance in a similar way as DR hybrids [9]. DT nucleotides were found to be in *anti* conformation in regard the glycosidic bond [12], but otherwise very little is known regarding their base-pair formation such as its hydrogen bonds and stacking interactions. Recently, we established a mesoscopic model to infer some of the structural information of oligonucleotides from melting temperatures, for instance we were able to show the stronger hydrogen bond in RNA [13], and also modelled DR [4] where we confirmed the deoxypyrimidine dependence on thermal stability. Here we apply the mesoscopic model to study the hydrogen bonds and stacking interactions for the DT hybrids based on melting temperatures.

The mesoscopic approach we use is the Peyrard-Bishop (PB) model [14], a simplified way to include the two main intra-molecular interactions of oligonucleotide duplexes which are the hydrogen bonds and stacking parameters. The PB model has found numerous applications, such as modelling G-quadruplexes [15], chaotic properties of promoter sequences [16], phonon modes [17] and DNA as a thermal transistor [18].

To calculate the melting temperatures we use an index calculated from the PB model and a correlation to measured temperatures [19]. We demonstrated that it is possible to run the model in reverse and to extract model parameters from the melting temperatures and in this way gain an insight of the intra-molecular interactions [20]. With the new parameters obtained in this way we are able to predict melting temperatures of new sequences and also calculate a qualitative opening profile of the double helix as function of temperature.

2. Materials and Methods

2.1. Notation

To facilitate the description about the hybrid DNA/TNA (DT) duplex, we introduce the usual notation dA, dC, dG and dT for DNA bases and tA, tC, tG and tG for TNA bases. This is then used

to describe the base pairs as dAtT, dTtA, dGtC and dCtG. The nearest-neighbor model allows us to define

Note that due to symmetry considerations, dTtA-dAtT is same as tTdA-tAdT. Therefore, for simplicity, we always use the notation starting with deoxy. When grouping in terms of purine or pyrimidine bases, we use the notation dR (tR) for dA, dG (tA, tG) and dY (tY) for dT, dC (tT, tC). Note that some authors use Pu for R, and Py for Y.

2.2. Melting temperature data set

In this work, we use 8 DT sequences and melting temperature data set from Schöning et al. [1], 14 from Lackey et al. [3] and 3 new as yet unpublished sequences, all at 1.0 M NaCl, 10 mM NaH₂PO₄, 0.1 mM EDTA, pH = 7.0 and at strand concentration C_t of 10 μ M. The new sequences were synthesized and measured under the same conditions as in Ref. 3. The complete list of sequences is shown in the table 1.

2.3. Mesoscopic model

The Peyrard–Bishop (PB) model is a physical statistical model, in which the potential for describing the hydrogen bonds of two bases on opposite strands is a Morse potential [14], which defined for *i*th base pair as $V(y_i) = D_{\alpha} \left(e^{-y_i/\lambda_{\alpha}} - \frac{1}{2} \right), \tag{2}$

where the parameter D_{α} represents the strength of the potential and λ_{α} is the potential width of a base-pair of type α . The stacking interaction between two neighboring base pairs is described by a harmonic potential, modified to consider a small twist angle θ [19, 20]

$$W(y_{i}, y_{i-}) = \frac{k_{\beta}}{2} \left(y_{i}^{2} - 2y_{i}y_{i-} \cos \Theta + y^{2} \right), \tag{3}$$

where k_{β} is the coupling constant of nearest neighbors of type β , and the angle is fixed at $\theta = 0.01$ rad. We did not use a anharmonic potential [21] as this would only increase the number of parameters without improving the parameter optimization, as shown in Ref. [20]. Nevertheless, the new parameters can be used together with the anharmonic potential without problems.

Table 1: DNA/TNA sequences used in this work, of which only the TNA strand is shown, from 3° to 2° . T_i are the measured, and T_i° the calculated melting temperatures in °C. The experimental temperatures T_i were obtained from the references indicated, those marked with * are reported in this work.

Sequence	Reference	T_i	T_i	Sequence	Reference	T_i	T_i
t(TTTTTTTTTTTTTTT)	1	32	32.1193	t(CTTACGCT)	3	22.8	21.2382
t(TAATAATATAAATTTT)	1	47	42.755	t(AGTCCTGA)	3	20	21.2645
t(TTTTAAATATAATAAT)	1	43	42.755	t(CTGAGTCC)	3	22.9	21.7645
t(CGCTGAAT)	1	25	27.1983	t(GAGCCGTG)	3	40.8	40.0352
t(AAAAAAAAAAAAAAA)	1	68	68.0211	t(GCCGTGAG)	3	39.9	40.0352
t(AAAATTTATATTATTA)	1	41	40.7773	t(ACGTCATTCCTC)	3	44.6	44.9676
t(ATTATTATATTTAAAA)	1	36	40.7773	t(GCAATGTTCAGC)	3	51.1	52.014
t(ATTCAGCG)	1	26	23.9367	t(GCTGAACATTGC)	3	51	49.5808
t(AGATACAA)	3	25.2	25.3398	t(GAGGAATGACGT)	3	68.5	68.3511
t(AATACAGA)	3	25.1	25.3398	t(ATGGCGTGAC)	*	55	54.8502
t(AAGCGTAG)	3	36.1	35.5452	t(CGCCTGTCTAGAAGTT)	*	62	60.6895
t(AGCGTAAG)	3	35	35.5452	t(AACTTCTAGACAGGCG	*	63	64.8335
t(CTACGCTT)	3	20.3	21.2382				

With the two potentials of Eqs. (2) and (3) we can calculate the classical partition function from which we obtain an adimensional index τ_i , which is proportional to the melting temperatures. Additionally, we can calculate the average strand displacement (y_i) for each base pair i by calculating the expected value of y from the partition function [14, 22].

2.4. Calculation of melting temperatures

The measured melting temperatures T_i are linearly correlated to the melting index $\tau_i(P)$ within groups of sequences of length N and for a given set of parameters P. This correlation allows us to calculate the linear regression coefficients $a_0(N)$ and $a_1(N)$ from which we can predict the melting temperature $T_i(P)$ for any sequence

$$T_i(P) = a_0(N) + a_1(N)\tau_i(P),$$
 (4)

where $P = \{p_1, p_2, \dots, p_L\}$ is a set of L. The coefficients $a_{0,1}(N)$ follow a linear dependence with $N^{1/2}$

$$a_k(N) = b_{0,k} + b_{1,k} N^{1/2}, \quad k = 0, 1.$$
 (5)

2.5. Thermal equivalence optimization

For the same *i*th sequence there is difference between the measured temperature T_i and the predicted temperature $T_i(P)$ which depends on the parameter set P used to calculate the melting index $T_i(P)$. Our aim is to find a new set of parameters P that minimizes this difference

$$\chi_{i}^{2}(P_{j}) = \sum_{i=1}^{N} [T_{i} - T_{i}(P_{j})]^{2},$$
(6)

where P_j is the jth tentative set of parameters [20].

Another equation considered in our discussion is the average absolute melting temperature deviation

$$(\Delta T) = \frac{1}{N} \sum_{i=1}^{N} |T_i - T_i(P_j)|. \tag{7}$$

2.6. Minimization procedure

The challenge of minimizing Eq. (6) is to find the optimal set P which in the case of DT is comprised of 20 parameters, 4 Morse potentials and 16 stacking interaction potentials. The most important problem here is the occurrence of local minima of χ^2 and to overcome this a well tested approach is to perform the minimization procedure many times, each time starting from a different initial set of parameters, P_{init} .

Here, we start with the same generic parameters as used for DNA and RNA [13, 20], $D_{\text{dAtT}} = D_{\text{dTtA}} = 30 \text{ meV}$, $D_{\text{dCtG}} = D_{\text{dGtC}} = 80 \text{ meV}$, $\lambda_{\text{dAtT}} = \lambda_{\text{dTtA}} = 3.3333 \times 10^{-2} \text{nm}$, $\lambda_{\text{dCtG}} = \lambda_{\text{dGtC}} = 1.25 \times 10^{-2} \text{nm}$, and for all nearest-neighbors, $k = 2.5 \text{ eV/nm}^2$. We call this set the seed parameters, P_{seed} , and for each new minimization we choose new initial set P_{init} where each initial parameter is randomly chosen within $\pm 10\%$ of their corresponding seed parameters. The λ are kept at fixed values during all minimizations as we found that they have almost no influence over the final results [20], otherwise we would have to deal with yet another four parameters that would bring further difficulties for the convergence of the optimization procedure.

Initial minimization, D only. In this minimization, we start from the generic seed parameters and only calculate the Morse parameters D, while fixing all others. We calculated the minimization starting with 1000 different sets of initial parameters, and the best value of $n\chi^2$ found was 235 °C². The new Morse potentials were used as seed parameters for the next minimization step.

Second minimization, D and k. Here, we now calculated all parameters D and k, using as seed parameters the Morse potentials from the previous round. Again, we started with 1000 different sets of initial parameters around $\pm 10\%$ of the previous seed parameters. We then averaged the resulting D and k parameters and their quality parameters were $\chi^2 = 125$ °C² and $(\Delta T) = 1.8$ °C.

Third minimization, improving χ^2 . We use the parameters from the second minimization as new seed values and calculated again 1000 rounds for further optimization. The quality parameters were reduced to $\chi^2 = 67 \, ^{\circ}\text{C}^2$ and $(\Delta T) = 1.1 \, ^{\circ}\text{C}$.

Final minimization, estimate uncertainty. Lastly, we consider the influence of the experimental uncertainty on our optimized parameters. Instead of changing the initial parameters, we now

modify the melting temperatures by small random amounts such that the standard deviation from the original set is 0.5 °C. Considering 1000 rounds of minimizations, we obtain the final average values of D and k as well as their relative uncertainty. The final quality parameters changed little compared to the previous round, $\chi^2 = 66 \, ^{\circ}\text{C}^2$ and $(\Delta T) = 1.1 \, ^{\circ}\text{C}$.

2.7. Availability

The DT parameters calculated were included in the latest version of our free TfReg software [23] which can be used to verify our results. The software and the parameters are available at http://tinyurl.com/tfrequfmg.

3. Results and Discussion

For the numerical optimization of the 20 new parameters (4 Morse and 16 stacking potentials) we had only 25 independent sequences and melting temperatures. The limited data set is because TNA is not commercially available and is di**ffi**cult to synthesize, and that is why there is relatively little information about its hybridization properties. For a linear system this would clearly be su**ffi**cient, but for a nonlinear model it is harder to establish *a priori* if overfitting is avoidable. A clear sign of overfitting is when the average temperature deviation of (ΔT) results much smaller than the estimated experimental uncertainty. Fortunately, the resulting average temperature deviation was (ΔT) = 1.1 °C, which compared to a typical uncertainty of 0.5 °C, gives us confidence that numerical overfitting has not occurred. Note that for the nearest-neighbor model, the amount of required parameters is 32 (16 enthalpy and 16 entropy variations) and calculating these would not be possible for such a small amount of melting temperatures [24].

In table 2 we show the calculated Morse potentials, which can be associated to hydrogen bond strengths [20], for the DT hybrids. The TNA purine base (tR) clearly has a stabilizing influence as shown by the much stronger Morse potential of dTtA and dCtG over the pyrimidine base (tY), which suggest that this known purine dependence [3] is primarily due to hydrogen bonding. Note that dGtC with a tY base has a Morse potential which is barely larger than the dTtA base pair, which indicates that for certain applications there might be a problem discriminating between these types of base pairs. Also shown in table 2 are the Morse potentials we obtained for DR

Table 2: The parameter of Morse potential depth D optimized for DT hybrids, compared with previous results for related DR [4] base pairs. The standard deviation is displayed in parenthesis in compact uncertainty notation.

type	DT	D (meV)	type	DR	D (meV)
dYtR	dTtA	38.8(4)	dYrR	dTrA	40(2)
dRtY	dAtT	30.7(8)	dRrY	dArU	28(3)
dYtR	dCtG	53.5(5)	dYrR	dCrG	74(1)
dRtY	dGtC	42.0(3)	dRrY	dGrC	63(1)

hybrids in a previous work [4]. The comparison between the DT and DR Morse potentials shows two interesting results. First, the very close similarity of the dTtA and dAtT Morse potentials to their DR counterparts, indicating that the dT and dA bases accommodate really well to the TNA strand. This is consistent with the results from Pallan et al. [9] which observed this for dAtT and dTtA base pairs embedded in a B-DNA and A-DNA, respectively. However, the second result is probably more surprising: a comparatively weak Morse potential for the CG-type DT base pairs. Even the stronger dCtG potential falls well below the weaker DR dGrC potential. But the DT duplexes are generally not less stable than their DR equivalents, so how should we understand this results? As we will see next, it is the stacking potentials that will provide the additional stability.

The calculated stacking potential constants k are shown in table 3 and their values range between 1.48 eV/nm² for dCtG-dAtT to 3.77 eV/nm² for dAtT-dCtG. We found no correlation between the DT stacking potentials and their DR counterparts, which are also shown in table 3. Unlike the DR stacking potentials, which are quite small in some specific cases, we obtained no such weak potentials for DT. In fact, the higher DT stacking appears to counteract the weaker CG Morse potentials in several cases and provides for additional thermal stability.

The interplay of the various potentials within the nonlinear PB model is better appreciated by examining the average displacement profiles for some example sequences. Average displacement profiles are obtained from calculating the the expected value (y_i) of the y distance of Eq. (2) for the ith base pair [14]. These profiles can be interpreted as the expected base pair separation at

certain temperatures. Unfortunately, as the PB approach is a 2D model, some of the relevant degree of freedoms are absent from the thermodynamics and for very short sequences one has to set unrealistically low calculation temperatures. Note that this calculation temperature is unrelated to the melting temperatures calculated from Eq. (4). Therefore, the displacement profiles only give us a qualitative view of the expected base pair openings which, nevertheless, is helpful to understand the detailed influences the various potentials have over the stability of the duplex. In Fig. 1 we show six sequences adapted from table S1 of Ref. [25], all are hybridized to a probe DNA strand. The complementary DNA, RNA and TNA are target sequences which are either purine or pyrimidine rich. For DNA/DNA (DD) sequences, the purine content has little impact, as these are homoduplexes, as seen in Fig. 1a, at higher temperatures the displacement profiles are still very similar. The situation changes completely for DNA/RNA (DR), at higher temperatures the purine rich target sequence is much more stable (lower (y_i)), even more so than is DD equivalent, Fig. 1b. This purine/pyrimidine asymmetry is a well established property of DR hybrids [4, 26] and has important biological consequences [27]. For DT hybrids, the thermal stability shows a similar asymmetry to purine/pyrimidine content to DR as shown in Fig. 1c. However, unlike DR, the DT shows a much more flattened out profile. While it is easy to make out the CG base pairs from the opening profile for DR, for DT it is much harder to tell where the CG base pairs are from the profile alone. Another example is shown in Fig. 2 where we show sequences with varying deoxypyrimidine (dPy) content for DR and DT. The DR profiles show a characteristic bulged opening in the central positions due to AT or AU base pairs. In contrast, for equivalent DT sequences the profiles are almost flat, without any such pronounced features. Also, for 0% dPy (100% tPy) content the DT sequence shows much higher opening implying in a much weaker thermal stability, which correlates to a very large dissociation rates observed for large tPy content [25].

4. Conclusion

We calculated the mesoscopic parameters from DNA/TNA melting temperatures which can be associated to hydrogen bonding and stacking interactions. Our results confirm the expected asymmetry of the thermodynamic properties in regard to purine/pyrimidine content, similar to those of DNA/RNA hybrids. However, unlike DNA/RNA those the Morse potentials for CG base

Table 3: The parameter of harmonic potential, coupling constant k optimized for DT hybrids. The standard deviation is displayed in parenthesis in compact uncertainty notation. Also shown, for comparison are the equivalent stacking potentials of DR hybrid k_{DR} from Ref 4. All stacking potentials are given in eV/nm².

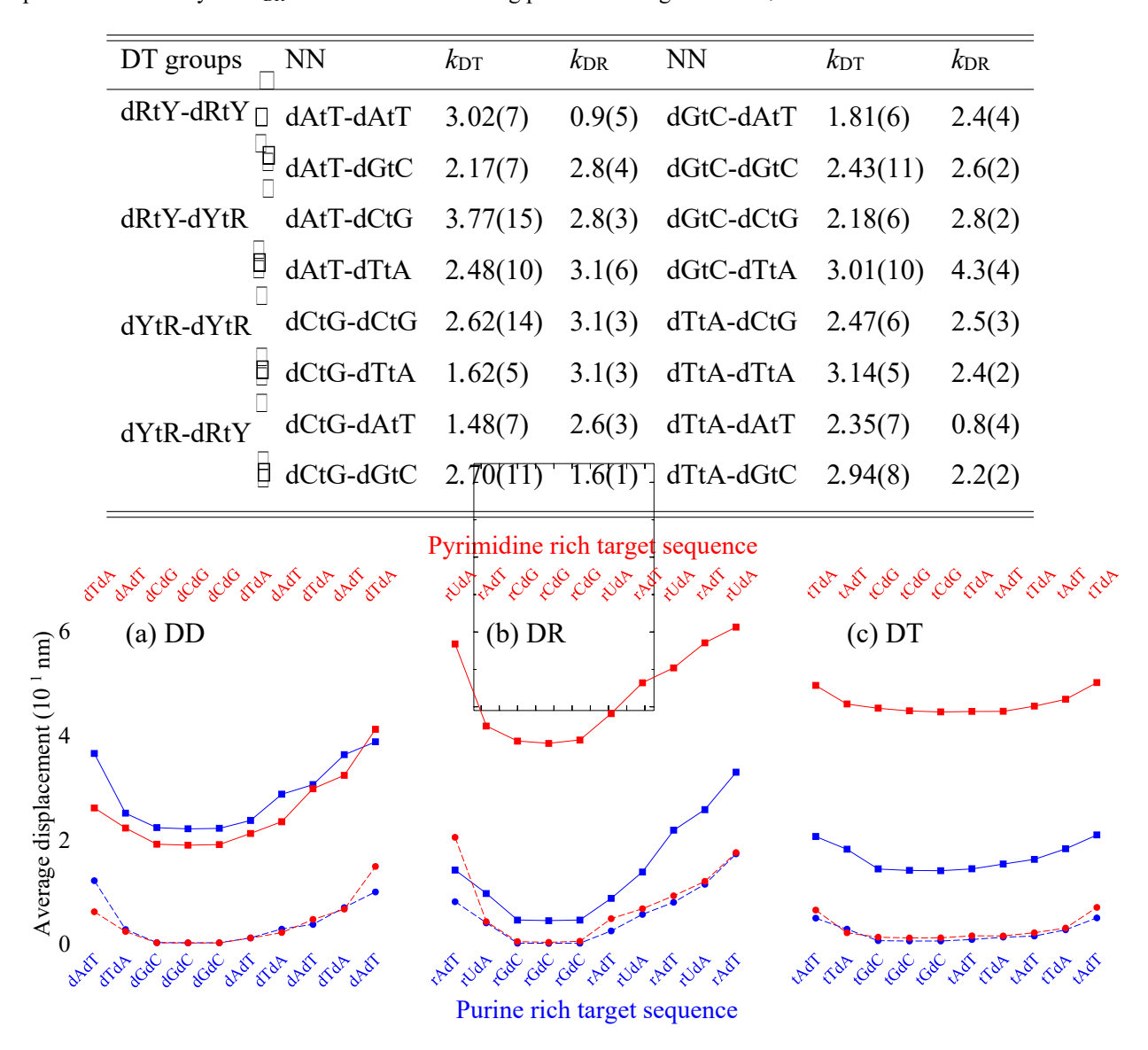


Figure 1: Temperature dependence of average displacement profiles for (a) DD, (b) DR and (c) DT purine rich (blue) and pyrimidine rich (red) targets adapted from Ref. 25. Bullets connected by dashed lines are for a calculation temperature of 150 K and squares connected by full lines are for 200 K.

pairs turned out very small for DNA/TNA. The consequence of these small potentials is that for DNA/TNA hybrids the duplex appears to dissociate much for uniformly and largely independent

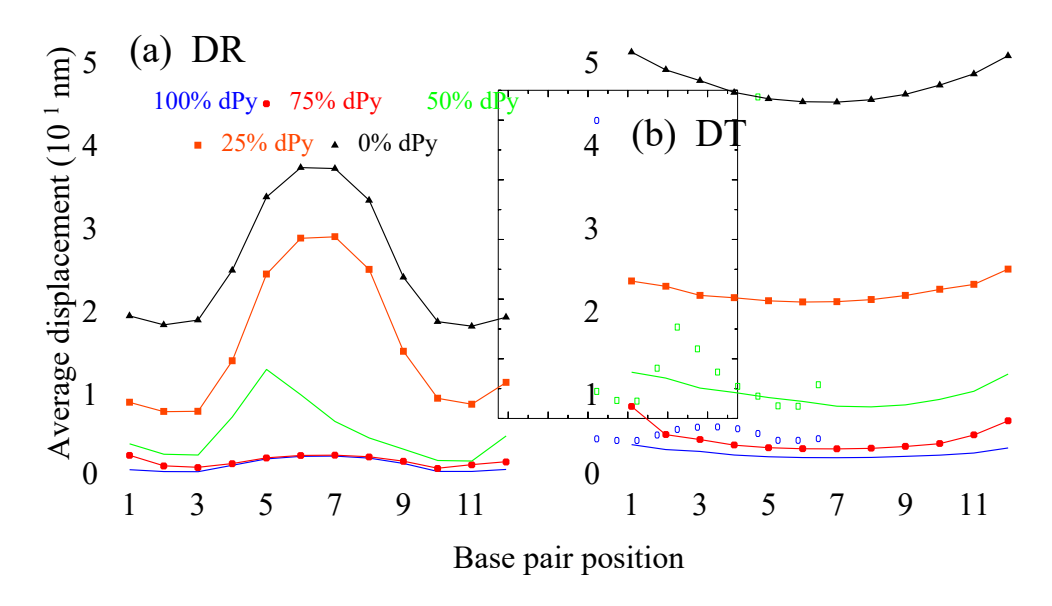


Figure 2: Average displacement profiles for (a) DR and (b) DT with varying deoxypyrimidine (dPy) content, calculated at 200 K. Sequences were adapted from Ref. 26, calculations for DR are from Ref. 4.

of sequence composition. As researchers continue to explore the use of TNA in synthetic biology and nanotechnology applications, these data provide important insight into the design of sequences and prediction of duplex stability.

Acknowledgements

MIM and GW were supported by Conselho Nacional de Desenvolvimento Cient´ıfico e Tecnológico (CNPq), Fundação de Amparo à Pesquisa do Estado de Minas Gerais (Fapemig) and Coordenação de Aperfeiçoamento de Pessoal de Nível Superior (Capes, Brazil, Finance Code 001). JMH was supported by the National Science Foundation (CHE-1904885). HHL received funding from the Air Force Institute of Technology Civilian Institute Program.

References

- [1] K.-U. Schöning, P. Scholz, S. Guntha, X. Wu, R. Krishnamurthy, A. Eschenmoser, Chemical etiology of nucleic acid structure: the α-threofuranosyl-(3¹ → 2¹) oligonucleotide system, Science 290 (5495) (2000) 1347–1351.
- [2] M. C. Culbertson, K. W. Temburnikar, S. P. Sau, J.-Y. Liao, S. Bala, J. C. Chaput, Evaluating TNA stability under simulated physiological conditions, Bioorg. Med. Chem. Lett. 26 (10) (2016) 2418–2421.
- [3] H. H. Lackey, E. M. Peterson, Z. Chen, J. M. Harris, J. M. Heemstra, Thermostability Trends of TNA:DNA Duplexes Reveal Strong Purine Dependence, ACS synthetic biology 8 (5) (2019) 1144–1152.
- [4] E. d. O. Martins, V.B. Barbosa, G. Weber, DNA/RNA hybrid mesoscopic model shows strong stability dependence with deoxypyrimidine content and stacking interactions similar to RNA/RNA, Chem. Phys. Lett. 715C (2019) 14–19, doi:10.1016/j.cplett.2018.11.015.
- [5] M. Salazar, O. Y. Fedoroff, J. M. Miller, N. S. Ribeiro, B. R. Reid, The DNA strand in DNA.RNA hybrid duplexes is neither B-form nor A-form in solution, Biochem. 32 (16) (1993) 4207–4215.
- [6] A. Noy, A. Pérez, M. Márquez, F. J. Luque, M. Orozco, Structure, Recognition Properties, and Flexibility of the DNA.RNA Hybrid, J. Am. Chem. Soc. 127 (13) (2005) 4910–4920.
- [7] P. Herdewijn, TNA as a potential alternative to natural nucleic acids, Angew. Chem., Int. Ed. Engl. 40 (12) (2001) 2249–2251.
- [8] Y.-W. Yang, S. Zhang, E. O. McCullum, J. C. Chaput, Experimental evidence that GNA and TNA were not sequential polymers in the prebiotic evolution of RNA, J. Mol. Evol. 65 (3) (2007)289–295.
- [9] P. S. Pallan, C. J. Wilds, Z. Wawrzak, R. Krishnamurthy, A. Eschenmoser, M. Egli, Why does TNA cross-pair more strongly with RNA than with DNA? An answer from X-ray analysis, Angew. Chem., Int. Ed. Engl. 42 (47) (2003) 5893–5895.
- [10] K.-U. Schöning, P. Scholz, X. Wu, S. Guntha, G. Delgado, R. Krishnamurthy, A. Eschenmoser, The α-L-Threofuranosyl-(3¹ → 2¹)-oligonucleotide System ('TNA'): Synthesis and Pairing Properties, Helv. Chim. Acta 85 (12) (2002) 4111–4153.
- [11] I. Anosova, E. A. Kowal, N. J. Sisco, S. Sau, J.-y. Liao, S. Bala, E. Rozners, M. Egli, J. C. Chaput, W. D. Van Horn, Structural insights into conformation differences between DNA/TNA and RNA/TNA chimeric duplexes, ChemBioChem 17 (18) (2016) 1705–1708.
- [12] C. J. Wilds, Z. Wawrzak, R. Krishnamurthy, A. Eschenmoser, M. Egli, Crystal structure of a B-form DNA duplex containing (L)-α-threofuranosyl (3¹ → 2¹) nucleosides: A four-carbon sugar is easily accommodated into the backbone of DNA, J. Am. Chem. Soc. 124 (46) (2002) 13716–13721.
- [13] G. Weber, Mesoscopic Model Parametrization of Hydrogen Bonds and Stacking Interactions of RNA from Melting Temperatures, Nucleic Acids Res. 41 (2013) e30, doi:10.1093/nar/gks964, URL http://nar.oxfordjournals.org/content/41/1/e30.
- [14] M. Peyrard, A. R. Bishop, Statistical Mechanics of a Nonlinear Model for DNA denaturation, Phys. Rev. Lett.

- 62 (23) (1989) 2755–2757.
- [15] A. Bergues-Pupo, F. Falo, A. Fiasconaro, Modelling the DNA topology: the effect of the loop bending on G-quadruplex stability, J. Stat. Mech.: Theory Exp. 2019 (9) (2019) 094004.
- [16] M. Hillebrand, G. Kalosakas, A. Schwellnus, C. Skokos, Heterogeneity and chaos in the Peyrard-Bishop-Dauxois DNA model, Phys. Rev. E 99 (2) (2019) 022213.
- [17] L. B. Alexandrov, K. Ø. Rasmussen, A. R. Bishop, B. S. Alexandrov, Evaluating the role of coherent delocalized phonon-like modes in DNA cyclization, Scientific Reports 7 (1) (2017) 9731.
- [18] S. Behnia, R. Panahinia, Molecular thermal transistor: Dimension analysis and mechanism, Chem. Phys. 505 (2018) 40–46.
- [19] G. Weber, N. Haslam, N. Whiteford, A. Prügel-Bennett, J. W. Essex, C. Neylon, Thermal Equivalence of DNA Duplexes Without Melting Temperature Calculation, Nat. Phys. 2 (2006) 55–59, doi:10.1038/nphys189.
- [20] G. Weber, J. W. Essex, C. Neylon, Probing the Microscopic Flexibility of DNA from Melting Temperatures, Nat. Phys. 5 (2009) 769–773, doi:10.1038/nphys1371.
- [21] T. Dauxois, M. Peyrard, A. R. Bishop, Entropy-driven DNA denaturation, Phys. Rev. E 47 (1) (1993) R44–R47.
- [22] Y.-L. Zhang, W.-M. Zheng, J.-X. Liu, Y. Z. Chen, Theory of DNA melting based on the Peyrard-Bishop model, Phys. Rev. E 56 (6) (1997) 7100–7115.
- [23] G. Weber, TfReg: Calculating DNA and RNA Melting Temperatures and Opening Profiles with Mesoscopic Models, Bioinformatics 29 (2013) 1345–1347, doi:10.1093/bioinformatics/btt133, URL http://bioinformatics.oxfordjournals.org/content/29/10/1345.
- [24] G. Weber, Optimization Method for Obtaining Nearest-Neighbour DNA Entropies and Enthalpies Directly from Melting Temperatures, Bioinformatics 31 (6) (2015) 871–877, doi:10.1093/bioinformatics/btu751, URL http://bioinformatics.oxfordjournals.org/content/31/6/871.
- [25] H. H. Lackey, Z. Chen, J. M. Harris, E. M. Peterson, J. M. Heemstra, Single-Molecule Kinetics Show DNA Pyrimidine Content Strongly Affects RNA:DNA and TNA:DNA Heteroduplex Dissociation Rates, ACS Synth. Biol. doi:10.1021/acssynbio.9b00471.
- [26] G. Suresh, U. D. Priyakumar, DNA–RNA hybrid duplexes with decreasing pyrimidine content in the DNA strand provide structural snapshots for the A-to B-form conformational transition of nucleic acids, Phys. Chem. Chem. Phys. 16 (34) (2014) 18148–18155.
- [27] S. Hamperl, K. A. Cimprich, The contribution of co-transcriptional RNA:DNA hybrid structures to DNA damage and genome instability, DNA Repair 19 (2014) 84–94.